A GLIMPSE of two massive circumstellar disks

C. Walker[1],K. Wood[1],B.A. Whitney[2], M. R. Meade,[3] B. L. Babler,[3] R. Indebetouw,[4] C. Watson,[5] M. G. Wolfire,[6] M. J. Wolff,[2] R. A. Benjamin,[7] D. P. Clemens,[8] T. M. Bania,[8] M. Cohen,[9] J. M. Dickey,[10] J. M. Jackson,[8] H. A. Kobulnicky,[11] J. S. Mathis,[3] E. P. Mercer,[8] S. R. Stolovy,[12] B. Uzpen,(11) E. Churchwell[3]

Received _____; accepted _____

To appear in ApJ.

[1]School of Physics & Astronomy, University of St. Andrews, North Haugh, St Andrews, KY16 9SS, Scotland; cw26@st-and.ac.uk

[2]Space Science Institute, 4750 Walnut St. Suite 205, Boulder, CO 80301

[3]University of Wisconsin-Madison, Dept. of Astronomy, 475 N. Charter St., Madison, WI 53706

[4]University of Virginia, Astronomy Dept., P.O. Box 318, Charlottesville, VA, 22903-0818

[5]Manchester College, Physics Dept., Box 117, North Manchester, IN 46962

[6]University of Maryland, Dept. Astronomy, College Park, MD 20742-2421

[7]University of Wisconsin-Whitewater, Physics Dept., 800 W. Main St., Whitewater, WI 53190

[8]Boston University, Institute for Astrophysical Research, 725 Commonwealth Ave., Boston, MA 02215

[9]University of California-Berkeley, Radio Astronomy Lab, 601 Campbell Hall, Berkeley, CA 94720

[10]University of Minnesota, Dept. Astronomy, 116 Church St., SE, Minneapolis, MN 55455

[11]University of Wyoming, Dept. Physics & Astronomy, PO Box 3905, Laramie, WY 82072

[12]Caltech, Spitzer Science Center, MS 314-6, Pasadena, CA 91125

ABSTRACT

We report the discovery of two objects in the *Spitzer* GLIMPSE survey that appear to be massive circumstellar disks. The image morphologies of the objects resemble those of scattered light disks around low mass T Tauri stars. However, the candidate disks are around 18″ and 36″ diameter and are very bright at IRAC wavelengths. Distances to the objects are unknown, but if they are associated with close by star formation within the IRAC field of view they may lie at distances greater than 1 kpc, implying disk radii of greater than 9 000 AU. If the objects are indeed large disks then our radiation transfer modelling requires that the central sources must have luminosities greater than $300\,L_{\odot}$ and estimated disk masses of tens of solar masses. Our modelling suggests that fluorescent emission from PAHs may be required to explain the brightness of the IRAC images, lending further support to the massive star plus disk hypothesis. Alternative explanations are that the objects are nearby smaller disks or just random wisps of interstellar material. We discuss further observations that will aid in determining if the objects are indeed large disks.

1. Introduction

The processes leading to the formation of high mass stars are currently poorly understood both observationally and theoretically. It is still open for debate whether massive stars form by accretion through a collapsing envelope and accretion disk like low mass stars or via mergers of lower mass stars in dense clusters. It had been thought for many years that the accretion scenario would not be possible since radiation pressure would halt the accretion flow (Kahn 1974; Yorke & Krügel 1977; Wolfire & Cassinelli 1987;

Beech & Mitalas 1994). However, recent radiation hydrodynamic models suggest that non-spherically symmetric systems may allow accretion to proceed through dense equatorial disks or tori which act as a shield to the intense stellar radiation field (Yorke & Sonnhalter 2002). Radiation transfer models also suggest accretion through a disk can be aided by the presence of protostellar outflows that reduce radiation pressure (Krumholz et al. 2005). Observationally there is mounting evidence for the accretion scenario with the detection of infall, outflow and equatorially flattened density structures in massive star formation regions (e.g., Zhang et al. 2002; Wu & Evans 2003; Fuller et al. 2005). In addition there are observations indicating the presence of circumstellar disks around massive stars (e.g., Zhang et al. 1998, 2002; Shepherd et al. 2001; Beltrán et al. 2004; Cesaroni et al. 2005; Beuther et al. 2005; Jiang et al. 2005; Patel et al. 2005), which are seen as a natural conduit for accretion.

Dusty circumstellar accretion disks are a key ingredient in the formation and evolution of low mass pre-main-sequence stars. They provide a channel for accretion of material onto the forming star; if coupled to the star by magnetic fields, may strongly influence the star's angular momentum evolution; and they are also the likely sites for planet formation. Studying and characterising circumstellar disks is therefore an important area of star and planet formation research.

The primary means for detecting disks around low mass T Tauri stars is through their signature infrared excess emission, over and above that from the stellar photosphere (e.g., Lada & Adams 1992). The last decade has also seen the imaging of T Tauri disks via scattered starlight (e.g., Burrows et al. 1996; Lucas & Roche 1997, 1998a,b; Padgett et al. 1999; Koresko 1998; Stapelfeldt et al. 1998; Jayawardhana et al. 2002) clearly revealing the flared structure and the dark, optically thick mid-plane regions predicted by radiation transfer simulations (Whitney & Hartmann 1992). Disks around the intermediate mass

Herbig Ae/Be stars have been inferred from infrared excesses and their disks appear to exhibit similar flaring structures to T Tauri disks (Dominik et al. 2003; Dullemond et al. 2001). There are also near IR and mid IR images of an edge-on flaring disk around a Herbig Ae binary star (Perrin et al. 2004).

In recent years evidence is starting to accumulate for circumstellar disks (or at least flattened structures) around stars even more massive stars than the Herbig Ae/Be stars. These observations suggest that massive stars may also form by the accretion of material through a disk in a similar manner to lower mass stars. Massive stars are more luminous at ultraviolet wavelengths than low mass stars, therefore an additional spectral feature that is available for study is the fluorescent excitation of PAHs in their circumstellar disks, resulting in prominent mid-infrared emission features (e.g., Peeters et al. 2004). Indeed, mid-infrared spectra of several Herbig Ae/Be stars are well explained with PAH fluorescence (e.g., Habart et al. 2004). In addition, recent high resolution mid-infrared images have revealed PAH fluorescence in a 900 AU diameter disk surrounding WL16 (estimated spectral type B8 to A0) in the ρ Ophiuchi cloud (Ressler & Barsony 2003).

The advent of the *Spitzer* Space Telescope provides another opportunity for high resolution mid-infrared imaging and spectroscopy to study PAHs in the circumstellar environment of massive stars. Preliminary results from the GLIMPSE survey shows that PAH emission in the IRAC images serves as a clear signpost for massive stars. Imaging at IRAC wavelengths will allow us to further investigate whether disks glowing in PAHs are a common feature in massive star formation. In this paper we present the first images from *Spitzer* that appear to show disks around massive stars. The bipolar morphology of the *Spitzer* images suggests the candidate disks are viewed close to edge-on and their increasing brightness towards the longer IRAC wavelengths is suggestive of PAH fluorescence. Using radiation transfer models, we explore the possibility that massive circumstellar disks can

explain the observed bipolar morphologies. Section 2 describes the observations and the image morphologies that lead us to identify the objects as candidate disks. Section 3 presents radiation transfer models for the images and infrared spectral energy distributions. Section 4 summarizes our findings and discusses follow-up observations required to further probe the disk hypothesis.

2. Observations

This section presents the GLIMPSE discovery images of the two disk candidates and details of the observations and data reduction. The local environment of each candidate is discussed along with the evidence suggesting the objects may be disks.

2.1. Disk Candidates

The two objects, hereafter referred to as A and B, which we identify as candidate circumstellar disks are shown in Fig. 1 and Fig. 2. The figures show near infrared images from the 2MASS survey along with the IRAC discovery images. The longest wavelength IRAC images at 8μm of both objects show a bipolar morphology. This morphology is reminiscent of observations and simulations of high inclination scattered light disks around T Tauri stars where the dense mid-plane regions create a dark lane bisecting the scattered light nebula and blocking direct light from the central source (Whitney & Hartmann 1992; Burrows et al. 1996). Scattered light disks around T Tauri stars are observed to have diameters in the range 100 AU to 600 AU and in the nearby Taurus-Auriga association the angular diameters are a few arcseconds at most. In contrast, the IRAC images in Figures 1 and 2 show nebulae that are $\sim 18''$ and $\sim 36''$ across, which if at the Taurus-Auriga distance of 140 pc (Elias 1978; Kenyon et al. 1994) would imply disk diameters of thousands of AU.

However, as discussed below, we believe these two objects may lie at even greater distances of around 1 kpc to 2 kpc, resulting in disk diameters greater than 9 000 AU. If these objects are disks around young stars they may be the largest yet discovered. Before discussing the individual objects in more detail, we first describe the data acquisition and reduction procedures.

2.2. Observations and Data Reduction

The co-ordinates, observation dates, and *Spitzer* observation identification number for objects A and B are given in Table 1. The mid-infrared observations were made as part of the GLIMPSE survey, using the Infrared Array Camera (IRAC) (Fazio et al. 2004) on the *Spitzer* Space Telescope (Werner et al. 2004). Data was obtained in all four IRAC bands (central wavelengths of 3.6μm, 4.5μm, 5.8μm, and 8.0μm). For object A these observations were taken on 3/11/04 (Spitzer Program ID 9225216), and were processed by the *Spitzer* Science Center (SSC) Pipeline (version S9.5.0). For object B these observations were taken on 3/4/04 and 7/21/04 (Spitzer Program ID 9225216 and 11768832) and were processed by the *Spitzer* Science Center (SSC) Pipeline (version S9.5.0 and S10.5.0). The data were further processed by the GLIMPSE pipeline to remove instrumental artifacts such as column pulldown and banding (Hora et al. 2004). Positional accuracies are better than 1″ (Werner et al. 2004) and the pixel size in the IRAC images is 0.6″. Point source full-width-half-maximum resolutions range from $\simeq$ 1.6″ at 3.6μm to $\simeq$ 1.9″ at 8μm. Every part of the sky in the GLIMPSE survey was observed twice with an exposure time of 1.2 seconds. Mosaic images, which conserve surface brightness, were created using the Montage package[1].

[1]available at http://montage.ipac.caltech.edu

Near-IR images of objects A and B at the J, H, and K bands were obtained from the 2MASS[2] survey. Fluxes were extracted from the IRAC and 2MASS images using aperture photometry routines. We estimate the flux calibration of these images is accurate to within 7%, based on comparisons of spectral synthesis models with observations of early A-type dwarf stars in the GLIMPSE survey (Cohen et al. 2003).

2.3. Local Environments and Distance Estimates

While the IRAC images in figures 1 and 2 resemble scattered light disks, it is instructive to place the objects in a broader context with images that show the large scale environments in which they reside. This is done in Figure 3 for object A and Figure 4 for object B. These figures show mosaic three color images (3.6μm, 5.8μm, and 8μm) with a 0.3×0.3 degree field of view. We immediately see that both objects show similar brightness levels compared with the surrounding field. As stated in the introduction, bright emission in IRAC images is common in regions containing massive stars and is often attributed to the presence of polycyclic aromatic hydrocarbons (PAHs) that have been stochastically heated by UV photons (e.g., Uchida et al. 1998; Li & Draine 2002). One possible source for the UV flux is from massive star formation (e.g., Peeters et al. 2004), which is often accompanied with clusters of low mass stars.

Both objects are in the sightline of the inner Sagittarius spiral arm and if they are associated with star formation within it their distances could be in the range 1 kpc to 2 kpc (Becker & Fenkart 1970). The presence of ionized gas (Bronfman et al. 1996; Kuchar &

[2]The Two Micron All Sky Survey is a joint project of the University of Massachusetts and the Infrared Processing and Analysis Center/California Institute of Technology, funded by the National Aeronautics and Space Administration and the National Science Foundation.

Clark 1997; Paladini et al. 2003), radio emission (Caswell & Haynes 1987, Cohen - private communication), and molecular gas (Avedisova (2002) and references therein) all lend support to active star formation in the field of object A. The field of object B appears sparser than that of object A and the nearest previously identified star formation region is located around 10′ away (Avedisova 2002). If these objects are young with circumstellar disks they would be expected to be associated with nebulae or open clusters (regions where star formation is or has very recently taken place) and therefore object A presents itself as the more convincing pre-main sequence disk candidate. It is also possible these are more evolved objects as there is at least one notable observation of an optically thick disk with radius $\sim 10\,000$ AU in the proto-planetary nebulae known as Gomez's Hamburger (Ruiz et al. 1987).

2.4. Image Brightness and Morphology

The small scale IRAC images of object A and B show that the bipolar disk-like morphology is brightest in the 8μm images. The increasing surface brightness toward longer wavelengths is a tell-tale signature of PAH fluorescence and/or emission from very small grains. Note that the 4.5μm IRAC band does not contain any strong PAH emission features (Peeters et al. 2004), and consequently it exhibits a lower surface brightness than the other IRAC bands. At near-IR wavelengths the 2MASS images of object A show a hint of bipolar morphology at K, but just an unresolved source at J and H. For object B the bipolar disk-like morphology is not present at wavelengths shorter than 5.8μm and foreground sources contaminate the nebulosity at wavelengths shorter than 8μm. The JHK bands do not contain prominent PAH emission, so if these objects are circumstellar disks the JHK images would be dominated by scattered starlight which is likely to be much fainter than the longer wavelength PAH emission. Deeper near-IR imaging is therefore required to

determine if the objects exhibit the signatures of scattered light disks at JHK. We will discuss this at greater length in the modelling sections below.

3. Models

3.1. Radiation Transfer Simulations

We firstly use our Monte Carlo radiation transfer code to generate radiative equilibrium models. These models do not currently include non-equilibrium heating and emission from small dust grains or PAHs (see Misselt et al. (2001) for an example of a Monte Carlo code that does include these effects). We then use a modified Monte Carlo scattered light code to generate approximate PAH fluorescent models which allow us to examine the qualitative morphology of PAH fluorescence in disks.

We model the images and spectral energy distributions using our Monte Carlo radiation transfer code. This code calculates radiative equilibrium temperatures, multi-wavelength images and spectra for dusty circumstellar disks and envelopes illuminated by a central source. The radiative equilibrium algorithm is described in Bjorkman & Wood (2001) and further code details and capabilities are presented in Wood et al. (2002a,b) and Whitney et al. (2003a,b). For the radiative equilibrium models we make the assumption that the image morphology seen in the IRAC 4.5μm band is dominated by thermal reprocessed radiation and has negligible emission from small grains and PAHs. The dust model we adopt is described in Wood et al. (2002b) and is one we have used to model the SEDs of several T Tauri disks. It provides a good match to long wavelength thermal SEDs ($\lambda > 200\mu$m) and has a grain size distribution that extends to larger grain radii than interstellar grain models. The PAH spectra presented in Peeters et al. (2004) show that the 4.5μm IRAC band does not contain strong PAH emission, but the emission contribution

from the small grain continuum may be important (see models in Misselt et al. (2001)). Our radiative equilibrium models for object A are tuned to fit the 4.5μm IRAC flux and image morphology and as a result may not fit the other IRAC bands where PAH emission is important. For object B, we only attempt to fit the image morphology at 8μm due to the severe contamination by foreground sources at shorter wavelengths. Therefore, because the 8μm images are bright in PAH emission our dust radiative equilibrium models for object B likely overestimate the source luminosity. All models presented below are for disks heated solely by radiation from the central star and we adopt blackbody input stellar spectra.

As discussed above, the image morphologies of the IRAC images for objects A and B resemble scattered light disks. The PAH fluorescent process can be modelled qualitatively using modified Monte Carlo scattering codes where UV source photons are absorbed by PAHs and reprocessed to optically thinner mid-IR wavelengths. We have therefore constructed qualitative PAH fluorescent models using a modified scattered light code as follows. Source photons are emitted and the dust opacity and scattering properties (opacity, albedo, and scattering phase function asymmetry parameter) are set to be those appropriate for a dust mixture incorporating PAHs at ultraviolet wavelengths: $\kappa = 404.4\mathrm{cm}^2\,\mathrm{g}^{-1}$, $a = 0.5823$, $g = 0.5570$ (we assume the scattering may be represented by the Henyey & Greenstein (1941) phase function). These values are taken from Bruce Draine's webpage[3]. and are calculations from Draine (2003) for $\lambda = 3019\mathring{A}$, $R_v = 3.1$. a gas/dust ratio of 123.6 and a C abundance in PAHs relative to H of 55.8 ppm. If an ultraviolet source photon (really a photon energy packet) is absorbed by PAHs, a fraction of its energy will be reprocessed into the PAH emission features present at IRAC wavelengths. The relative probabilities of re-emitting a Monte Carlo energy packet at IRAC wavelengths are 2%, 2%, 17%, 79% for IRAC bands 1, 2, 3, 4 respectively based on the direct integration of

[3]http://www.astro.princeton.edu/∼draine

the Orion PAH spectrum from Peeters et al. (2004). We simulate this by isotropically re-emitting the absorbed photons from their point of absorption and setting the dust properties for the subsequent radiation transfer of the simulated fluorescent PAH photons to be those at the appropriate IRAC wavelength with properties are taken from our assumed circumstellar dust model: IRAC band 1 - $\kappa = 9.67\mathrm{cm}^2\,\mathrm{g}^{-1}$, $a = 0.285$, $g = 0.147$; IRAC band 2 - $\kappa = 6.16\mathrm{cm}^2\,\mathrm{g}^{-1}$, $a = 0.187$, $g = 0.085$; IRAC band 3 - $\kappa = 3.87\mathrm{cm}^2\,\mathrm{g}^{-1}$, $a = 0.111$, $g = 0.015$; IRAC band 4 - $\kappa = 5.01\mathrm{cm}^2\,\mathrm{g}^{-1}$, $a = 0.027$, $g = 0.05$. With this algorithm we can qualitatively examine the morphology of PAH fluorescence in disks and compare with simulated images from our radiative equilibrium dust codes that do not include PAH emission.

3.2. Circumstellar Density Structure

We adopt the following parameterization for the two dimensional density structure of flared disks (e.g., Shakura & Sunyaev 1973)

$$\rho = \rho_0 \left(\frac{R_\star}{\varpi}\right)^\alpha \exp -\frac{1}{2}[z/h(\varpi)]^2 \,, \tag{1}$$

where ω is the radial coordinate in the disk mid-plane and the scaleheight increases with radius, $h = h_0\,(\varpi/R_\star)^\beta$. For this set of models we also assume that dust in regions close to the star is destroyed if temperatures rise above 1600K (Duschl et al. 1996). Any remaining gas we assume to be optically thin and therefore we effectively have an opacity gap in the disk (e.g., Lada & Adams 1992). The disk is sharply truncated at this inner edge. We calculate simulated SEDs, thermal images (convolved with the appropriate IRAC spectral response curve), and simulated PAH fluorescent images as described above. We vary disk inclination, mass and scaleheight h_0 in an attempt to model the observed 4.5μm image morphology of object A and the 8μm morphology of object B. To minimize the large parameter space, we have fixed the parameters $\beta = 1.25$ and $\alpha = 2.25$ which are appropriate

for irradiated disks around low mass stars (D'Alessio et al. 1999), giving a surface density $\Sigma \sim \varpi^{-1}$.

Accretion disks around classical T-Tauri stars are typically a few hundred AU in radius with masses in the range 10^{-4} to $10^{-1}\,M_{\odot}$ (e.g., Calvet et al. 2000; Natta et al. 2000). Accretion disks around higher mass stars are not well understood, however there is evidence to suggest they can have masses of the order of the stellar mass (e.g., Cesaroni et al. 1997; Zhang et al. 1998), but also be larger than their lower mass counterparts so that densities are not necessarily higher. We estimate the minimum diameter of object A to be $\sim 18''$ and object B to be $\sim 36''$, which would give a considerable physical radius for both "disks" if they are located beyond a few tens of parsecs. If the objects are in the Sagittarius spiral arm, they may be up to 2 kpc distant, implying radii of tens of thousands of AU. In our models presented below we therefore consider two alternatives: (1) the objects are associated with star formation in the Sagittarius spiral arm at a distance of 1.6 kpc and are very large disks; (2) the objects are located much closer and have smaller disk radii more comparable with a low mass star.

3.3. Object A

For the radiative equilibrium models of object A we adopt disk radii of 1 000 AU and 20 000 AU, which correspond to distances of roughly 70 pc, and 1.6 kpc when compared to the observations. Stellar parameters, disk mass, scaleheight, and inclination are adjusted to provide a match to surface brightness and morphology. The best fit models are summarized in Table 3 and shown in Figs. 5 and 6. Many models were attempted in which we varied the disk parameters to fit by eye the overall image morphologies. In a more quantitative comparison, we compared surface brightness levels and took vertical cuts bisecting the bipolar nebulae to compare the shape and flux levels in the data and models. We feel that

a more detailed modeling analysis is not justified and should be saved for modeling any follow up observations that could confirm the disk hypothesis.

To make a comparison between our models and the IRAC images we find it is important to account for the foreground/background emission that is evident in the observations (see Fig. 3). For object A this emission is typically around 5% to 20% of the average surface brightness of the bipolar nebula. Adding a uniform background of this level to our simulations has a dramatic effect on the model images: masking the lower level outer regions of the model disks and making the upper bipolar lobe more prominent and rounder when compared to models without any simulated background emission. This is illustrated in Fig. 5a and Fig. 5b which respectively show one of our model images convolved with a Gaussian PSF to simulate the IRAC resolution, and the final product that has a uniform background added prior to the PSF convolution. All the model images in Fig. 6 have a background added and the addition of background emission improved fits to the observations. Figure 6 contains the IRAC 4.5μm data in both image and cross-section format for comparison with our models. The cross-sections perpendicular to the disk show general agreement between models and data.

Once we had found radiative equilibrium models that reproduced the image surface brightness and morphology at 4.5μm, we then investigated how these models compared to data at other wavelengths. We were unable to find a model that reproduces the observed surface brightness at all IRAC wavelengths. This discrepancy in part could be due to the properties of the dust we use, however as there is considerable background emission in all IRAC bands throughout the region in which this object is found we suggest there may be a significant contribution from PAHs and small grains. As stated previously, PAHs and small grains will be particularly strong at IRAC bands 1, 3 and 4. In the case of the 20 000 AU model disk, which we find requires a stellar luminosity $L_\star \sim 300 L_\odot$ (corresponding to a

main sequence spectral type of $\sim$ B7 [Cox 2000]), the star itself could provide the UV and optical photons required for non-equilibrium PAH heating. The inference of strong PAH/small grain emission makes the nearby small disk model unlikely, because the lower temperature central source will not provide enough UV luminosity to excite the PAHs. External illumination is not an alternative for the small disk because the image morphology of an externally illuminated disk does not exhibit the dark dust lane of internally illuminated models.

Based on our simulated images and the likely presence of PAHs/small grain emission, we believe that despite the unusually large disk the high luminosity model is the more likely. This is supported by the spectral energy distribution shown in Fig. 7 which shows the radiative equilibrium model SEDs and flux measurements for object A. Although the 1 000 AU disk provides a reasonable match to the morphology of object A it requires a large extinction ($A_V = 17$) to match the H and K flux measurements, highly implausible at a distance of 70 pc. The 20 000 AU model on the other hand only requires an $A_V = 6.2$, which we consider to be reasonable at a distance of 1.6 kpc for this sightline (Neckel & Klare 1980).

It is also clear from Fig. 7 that a match is not achieved at IRAC bands 1, 3, and 4, possibly due to the absence of PAH/small grain emission in our models. To test that PAH fluorescence can produce images that qualitatively match the IRAC data, we have constructed simulated PAH fluorescent images using the modified Monte Carlo scattering code described above. Figure 8 shows the simulated PAH fluorescent images and cross-sections for the same disk density structure from the models in Fig. 6. The approximate PAH model images show disks that are slightly more flared than the earlier models. This is due to the UV optical depth τ=1 surface being at a larger height above the mid-plane so that UV photons are absorbed, and reprocessed, at larger heights than stellar

photons in radiative equilibrium simulations. The image morphology is very similar to the data, showing that PAH fluorescence is indeed a plausible explanation for the IRAC data. Inclusion of PAH/small grain emission in our Monte Carlo codes is clearly required for more detailed models of these sources. However, the models presented here demonstrate that the data is consistent with our interpretation of large disks irradiated by a central source.

3.4. Results for Object B

For object B a single model for a disk of radius 20000AU is presented, corresponding to a source distance of 0.85 kpc. The choice of disk radius for object B is somewhat arbitrary as we are only attempting to fit the general morphology and not the fine details of this system. It does, however demonstrate once again that a large disk is required for source distances beyond tens of parsecs. Object B only has a clear bipolar structure in IRAC band 4. At wavelengths shorter than this foreground stars dominate the image. We modeled object B at 8μm to show that the general morphology of this object is characteristic of a highly inclined disk. Figure 9 shows an example model of a 20 000 AU disk inclined at $i = 85°$. This figure shows that a dark lane and two bright lobes, such as those evident in the observation of object B, are consistent with a very highly inclined model. Again adding a background, in this case 40% of the average surface brightness of object B, improves the fit to the shape of the object. This is a huge disk, however given a comparison with the observations it would only be located at approximately 850 parsecs. There is no recorded active star formation in the direction of object B and it seems most likely that any young star+disk system would be located in the spiral arm. For this to be the case object B would have to have an enormous disk well in excess of any known to date and for this reason we remain sceptical that this is a pre-main sequence circumstellar disk. One alternative explanation is that object B is not a disk, but is simply an optical illusion: it could just be

wisps of interstellar material illuminated by the ambient interstellar radiation field. We do not attempt to characterize this object further. If confirmed, these objects would be the most massive optically thick circumstellar disks detected.

4. Summary

We have presented new *Spitzer* observations from the GLIMPSE survey of two previously unidentified objects and have shown that the presence of highly inclined circumstellar disks could explain the bipolar morphology of these two objects. If these are disks associated with pre-main sequence objects they need to be either massive disks or very close by smaller disks. If object A lies at a distance of 70 pc, then we can reproduce the general morphology of the IRAC images with $M_d = 0.1 M_\odot$, $R_d = 1\,000$ AU, $i = 76°$ and a central source with $L = 0.64 L_\odot$, $T = 3\,500$ K. On the other hand, if it is associated with star formation in the Sagittarius arm and lies at a distance of 1.6 kpc, the image morphology is reproduced with $M_d = 40 M_\odot$, $R_d = 20\,000$ AU, $i = 73°$ and a central source with $L = 305 L_\odot$, $T = 14\,000$ K. The relative brightnesses of the IRAC images suggests that PAH fluorescence is important for accurately modeling the data. Using a modified Monte Carlo scattering code, we demonstrated qualitatively that PAH fluorescence can explain the IRAC image morphologies and relative brightnesses.

For object B foreground stars severely contaminate the images for wavelengths shorter than 8μm and we therefore only attempted to model the morphology of this object at 8μm. Assuming object B is at 0.85 kpc, its 8μm image morphology can be reproduced with $M_d = 34 M_\odot$, $R_d = 20\,000$ AU, $i = 85°$ and a central source with $L = 1754 L_\odot$, $T = 16\,000$ K. Due to the contamination from foreground sources, our identification of object B as a circumstellar disk is much more circumspect than for object A and the limited data does not warrant more detailed modeling efforts.

We found that foreground/background nebulosity is an important consideration in modeling these objects. Including a uniform foreground/background emission component in our radiation transfer simulations greatly improved the model fits. In the region of Object A the foreground/background emission is at the 5% to 20% level and for object B it is at the 40% level. The addition of foreground/background emission masks the outer, lower surface brightness regions of the disks, can change the relative prominence of the bipolar nebulosity, and makes the scattered light disk appear more rounded.

Although our modeling suggests that these objects may be massive circumstellar disks, the nebulae could simply be optical illusions that look like disks. A stability analysis indicates that our massive disk models have Toomre parameter $Q \ll 1$ at all radii. If the objects are disks, this would suggest they are gravitationally unstable and may be short lived. However, recent work by Lodato & Rice (2005) suggests that the phases of massive disks are not necessarily short when a more realistic treatment of disk thermodynamics is included in numerical simulations specifically if the disks are not assumed to be isothermal. Further observations are required to determine whether the objects are disks or just random wisps of interstellar dust. If images are formed by small disks casting a shadow on the cloud in which they are embedded, the cloud would need to be very flattened as models of this type produce much more extended morphologies (Hodapp et al. 2004). Deeper near infrared imaging at JHK could reveal the scattered light disks, which we expect to be much fainter than disks glowing in PAHs at the IRAC bands. Millimeter and radio interferometry could search for signatures of cold dust and whether the objects exhibit signatures of rotation.

We acknowledge financial support from a PPARC studentships (CW) and an Advanced Fellowship (KW). Support for this work, part of the *Spitzer Space Telescope* Legacy Science Program, was provided by NASA through Contract Numbers (institutions) 1224653 (UW), 1225025 (BU), 1224681 (UMd), 1224988 (SSI), 1242593 (UCB), 1253153 (UMn),

11253604 (UWy), 1256801 (UWW) by the Jet Propulsion Laboratory, California Institute of Technology under NASA contract 1407. This research made use of Montage, funded by the National Aeronautics and Space Administration's Earth Science Technology Office, Computational Technologies Project, under Cooperative Agreement Number NCC5-626 between NASA and the California Institute of Technology

REFERENCES

Avedisova, V. S., 2002, ARep, 46, 193

Becker, W., & Fenkart, R., 1970, in *The Spiral Structure of our galaxy*, IAU *symp.* No 38. Ed. W. Becker and G. Contopoulos, 205

Beech, M., Mitalas, R., 1994, ApJS, 95, 517

Beltrán, M. T., Cesaroni, R., Neri, R., Codella, C., Furuya, R. S., Testi, L., & Olmi, L., 2004, ApJ, 601, L187

Beuther, H., Zhang, Q., Sridharan, T. K., 2005, & Chen, Y., ApJ, 628, 800

Bjorkman, J. E., & Wood, K., 2001, ApJ, 554 , 615

Bronfman, L., Nyman, L.-Å., & May, J. 1996, A&AS, 115, 81

Burrows, C. J., et al. 1996, ApJ, 473, 437

Calvet, N., Hartmann, L., & Strom, S.E.,. 2000, in Protostars and Planets IV, ed. V. Mannings, A. P. Boss, and S.S. Russell (Tucson: Univ. Arizona Press), 377

Cardelli J. A., Clayton G. C., Mathis J. S., 1989, ApJ, 345, 245

Caswell, J. L., & Haynes, R. F., 1987, A&A, 171, 261

Cesaroni, R., Felli, M., Testi, L., Walmsley, C. M., & Olmi, L., 1997, A&A, 325, 725

Cesaroni, R., Neri, R., Olmi, L., Walmsley, C., & Hofner, P. 2005, A&A, 434, 1039

Cohen, M., Wheaton, W. A., & Megeath, S. T., 2003, AJ, 126, 1090

Cox, A. N. [ed.], 2000, Allen's Astrophysical Quantities (4th ed.; New York: Springer-Verlag)

D'Alessio, P., Calvet, N., Hartmann, L., Lizano, S., & Canto, J., 1999, ApJ, 527, 893

Dominik, C., Dullemond, C. P., Waters, L. B. F. M., & Walch, S., 2003, A&A, 398, 607

Draine, B. T., 2003, "Interstellar Dust Grains", Ann. Rev. Astr. Ap., 41, 241

Dullemond, C. P., Dominik, C., & Natta, A., 2001, ApJ, 560, 957

Duschl, W., Gail, H. -P., & Tscharnuter, W. 1996, å, 312, 624

Elias, J. H., 1978, ApJ, 224, 857

Fazio, G., et al. 2004, ApJS, 154, 10

Fuller, G. A., Williams, S. J., Sridharan, T. K., 2005, A&A, in press (astro-ph/0508098)

Habart, E., Natta, A., & Krügel, E., 2004, A&A, 427, 179

Henyey, L. G., & Greenstein, J. L., 1941, ApJ, 93, 70

Hodapp, K. W., Walker, C. H., Reipurth, B., et al. 2004, ApJ, 601, L79

Hora, J. L., et al. 2004, Proc. SPIE, 5487, in press

Jayawardhana, R., Luhman, K. L., D'Alessio, P., & Stauffer, J. R. 2002, ApJ, 571, L51

Jiang, Z., Tamura, M., Fukagawa, M., Hough, J., Lucas, P., Suto, H., Ishii, M., Yang, J., 2005, Nature, 437, 7055, 112

Kahn, F. D., 1974, A&A, 37, 149

Kenyon, S. J., Dobrzycka, D., Hartmann, L., 1994, AJ, 108, 1872

Koresko, C. D. 1998, ApJ, 507, L145

Krumholz, M. R., McKee, C. F., & Klein, R. I., 2005, ApJL, 618, L33

Kuchar, T. A., & Clark, F. O., 1997, ApJ, 488, 224

Lada C. J., Adams F. C., 1992, ApJ, 393, 278

Li, A., & Draine, B. T. 2002, ApJ, 572, 232

Lodato, G., Rice, W. K. M., 2005, MNRAS, 358, 1489

Lucas, P. W., & Roche, P. F. 1997, MNRAS, 286, 895

———. 1998a, MNRAS, 299, 699

———. 1998b, MNRAS, 299, 723

Misselt, K. A., Gordon, K. D., Clayton, G. C., & Wolff, M. J. 2001, ApJ, 551, 277

Natta, A., Grinin, V. P., & Mannings, V., 2000, in Protostars and Planets IV, ed. V. Mannings, A. P. Boss, and S. S. Russell (Tucson: Univ. Arizona Press), 559

Neckel T., & Klare G., 1980, AAS, 42, 251

Padgett, D., Brandner, W., Stapelfeldt, K. R., Strom, S. E., Terebey, S., & Koerner, D. 1999, AJ, 117, 1490

Paladini R., Burigana C., Davies R., Maino D., Bersanelli M., Cappellini B., Platania P., Smoot G., 2003, å, 397, 213

Patel, N. A., et al., 2005, Nature, 437, 7055, 109

Peeters, E., Spoon, H. W. W., & Tielens, A. G. G. M., 2004, ApJ, 613, 986

Perrin, M. D., Graham, J., R., Kalas, P., & Fitzgerald, M., 2004, AAS, 205, 127.01

Ressler, M. E., & Barsony, M., 2003, ApJ, 584, 832

Ruiz, M. T., et al., 1987, ApJ, 316, L21

Shakura N. I., & Sunyaev R. A., 1973, å, 24, 337

Shepherd, D. S., Claussen, M. J., & Kurtz, S. E., 2001, Science, 292, 1513

Stapelfeldt, K. R., et al. 1998, ApJ, 508, 736

Uchida, K. I., Sellgren, K., & Werner, M. 1998, ApJ, 493, L109

Werner, M. W., et al. 2004, ApJS, 154, 1

Whitney B. A., & Hartmann L., 1992, ApJ, 395, 529

Whitney, B. A., Wood, K., Bjorkman, J. E., & Wolff, M. J. 2003a, ApJ, 591, 1049

Whitney, B. A., Wood, K., Bjorkman, J. E., & Cohen, M. 2003b, ApJ, 598, 1079

Wolfire, M. G., & Cassinelli, J. P., 1987, ApJ, 319, 850

Wood K., Lada C. J., Bjorkman J. E., Kenyon S. J., Whitney B., Wolff M. J., 2002b, ApJ, 567, 1183

Wood K., Wolff M. J., Bjorkman J. E., Whitney B. A., 2002a, ApJ, 564, 887

Wu, J., & Evans, N. J., 2003, ApJ, 592, L79

Yorke H. W., & Krügel, E., 1977, A&A, 54, 183

Yorke, H. W., & Sonnhalter, C. 2002, ApJ, 569, 846

Zhang, Q., Hunter, T. R., & Sridharan, T. K., 1998, ApJ, 505, L151

Zhang, Q., Hunter, T. R., & Sridharan, T. K., & Ho, P. T. P., 2002, ApJ, 566, 982

This manuscript was prepared with the AAS LaTeX macros v5.2.

Table 1: Observation details

Object	Co-ordinates (J2000)	Date of Observations	Observation ID
A	14:25:16 -60:30:13	3/11/04	9225216
B	13:17:39 -62:27:04	3/4/04, 7/21/04	9228288, 11768832

Table 2: Model parameters

Model	$T_\star$ (10^3K)	$M_\star$ ($M_\odot$)	$R_\star$ ($R_\odot$)	M_d ($M_\odot$)	R_{in} ($R_\star$)	R_d (AU)	h0 ($R_\star$)	Inclination (degrees)	Comment
A.1	3500	0.4	2.2	0.08	5	1000	0.015	76	
A.2	14000	4	3	40	92	20000	0.01	73	
A.3	14000	4	3	40	92	20000	0.01	73	PAH approximation
B.1	16000	6	5.5	34	122	20000	0.01	85	

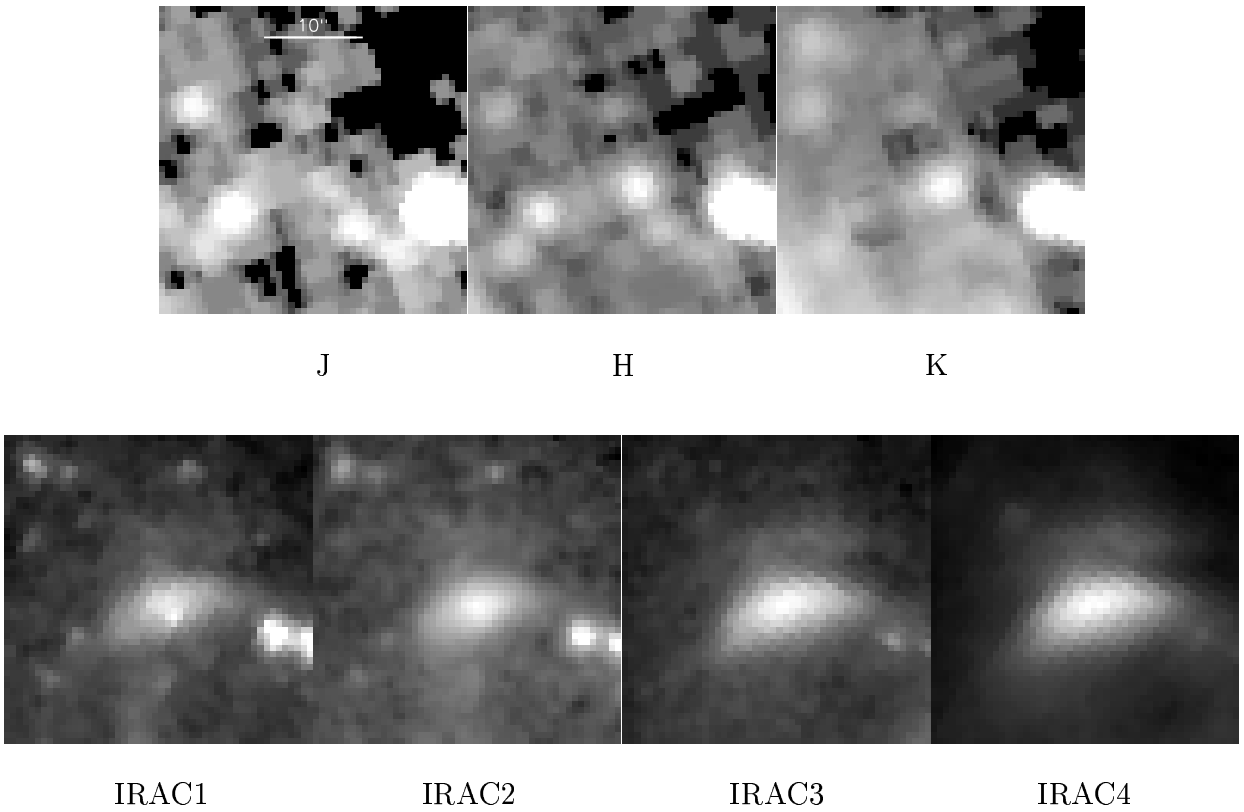

Fig. 1.— 2MASS JHK and IRAC band 1,2,3,4 images of object A stretched by a power of 0.3 and scaled to the object brightness. Images are 30″ on a side. Bipolar structure becomes less evident as wavelength of observation decreases.

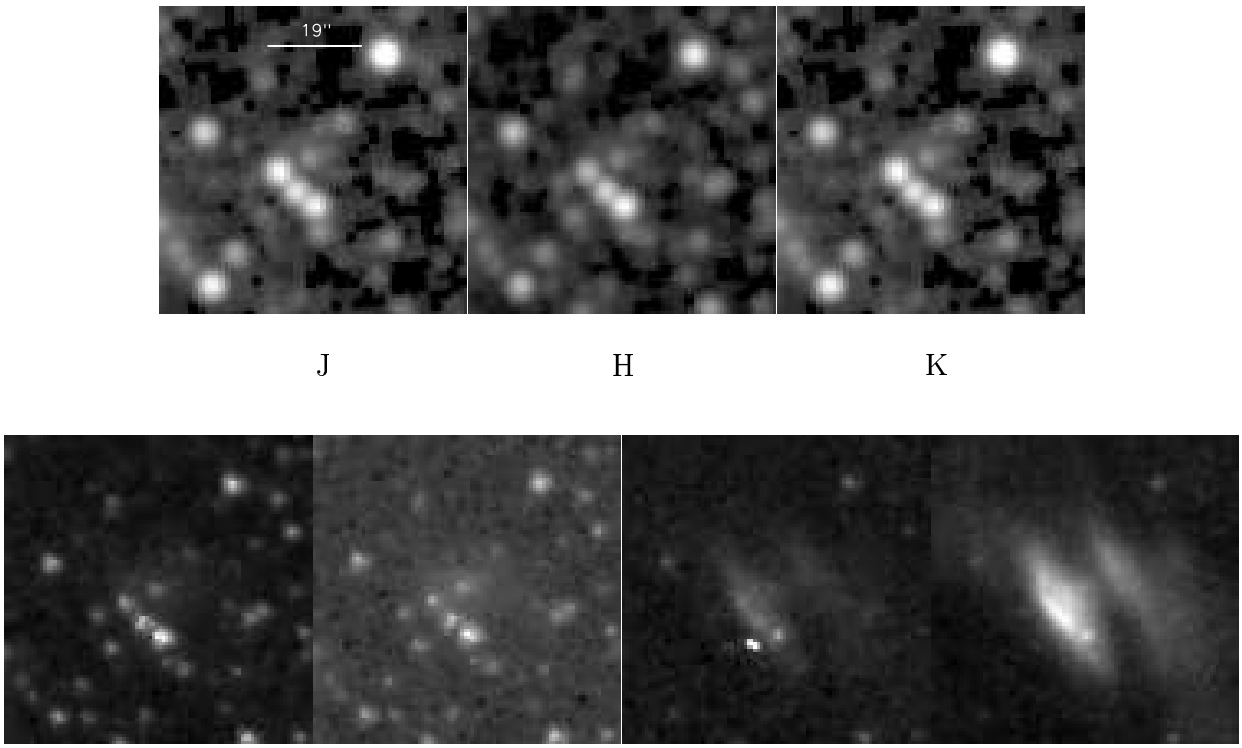

Fig. 2.— 2MASS JHK and IRAC band 1,2,3,4 images of object B stretched by a power of 0.3 and scaled to the object brightness. Images are 57″ on a side. Bipolar structure quickly disappears at wavelengths below IRAC band 4.

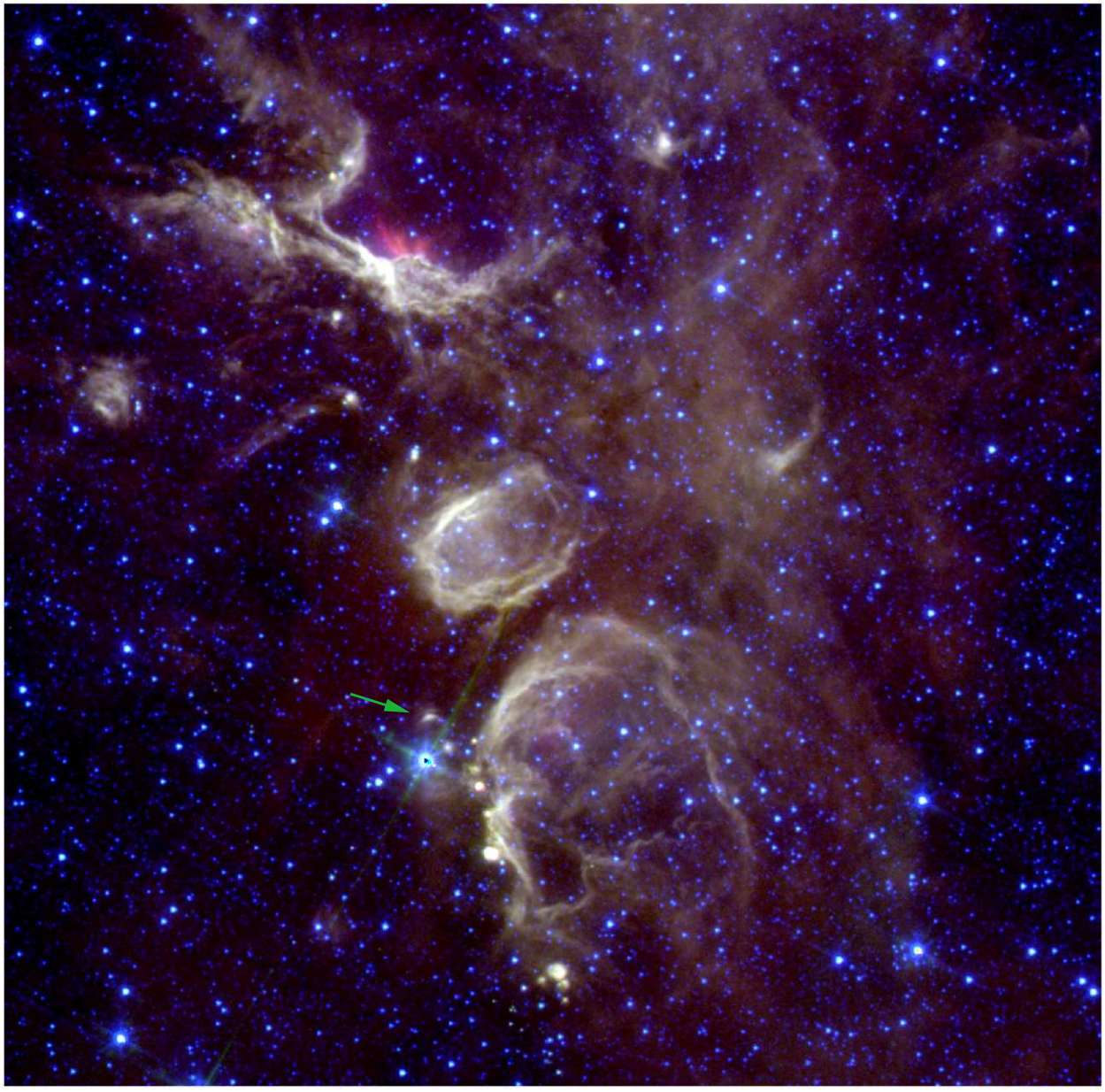

Fig. 3.— Three colour mosaics of IRAC band 1,3 and 4 images showing 0.3 × 0.3 degree field centred on object A at l=314.2, b=0.34. Image is aligned to galactic co-ordinates and scaled using histogram equalization.

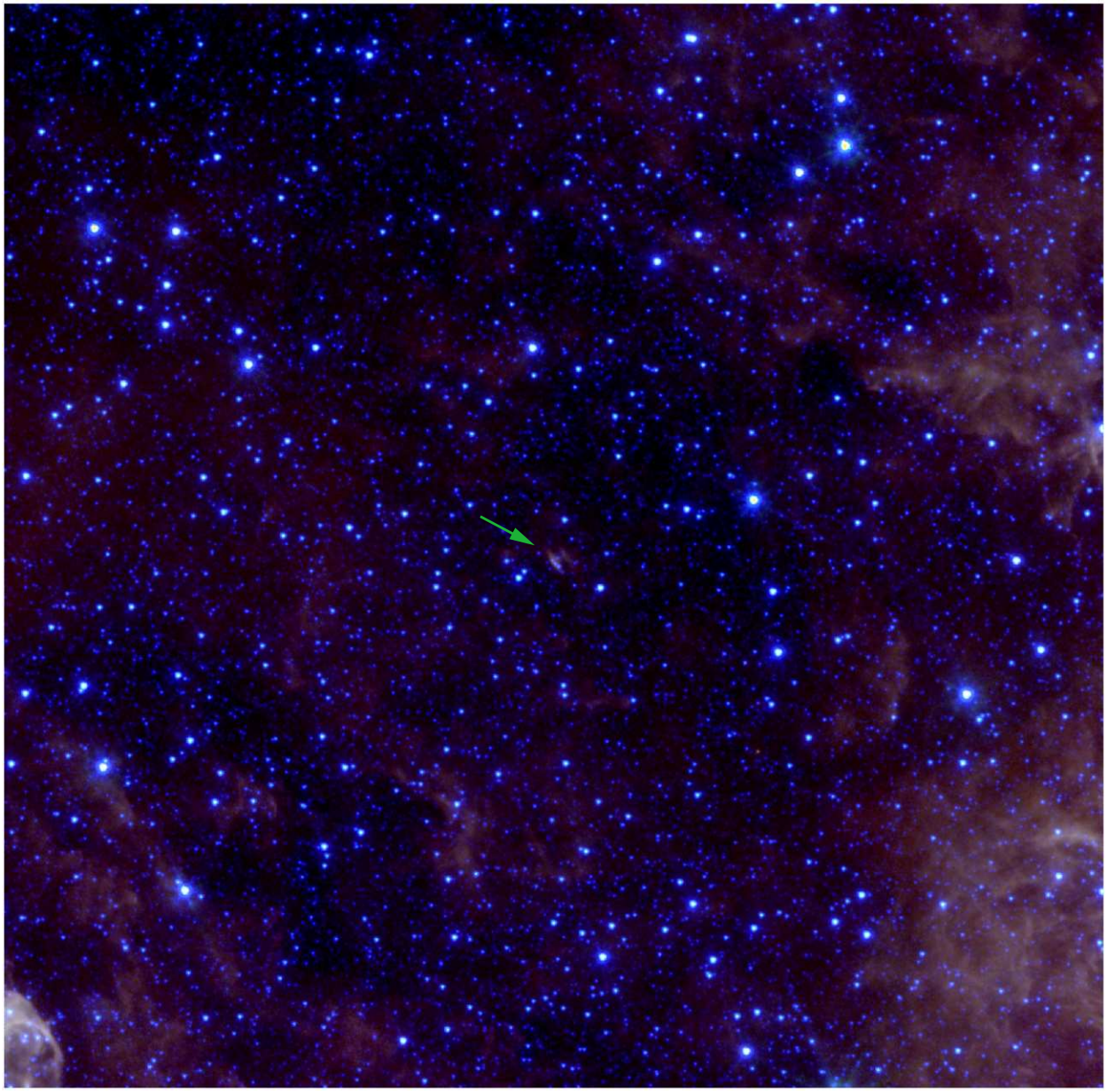

Fig. 4.— Three colour mosaics of IRAC bands 1,3 and 4 images showing 0.3 × 0.3 degree field centred on object B at l=305.96, b=0.34. Image is aligned to galactic co-ordinates and scaled using histogram equalization.

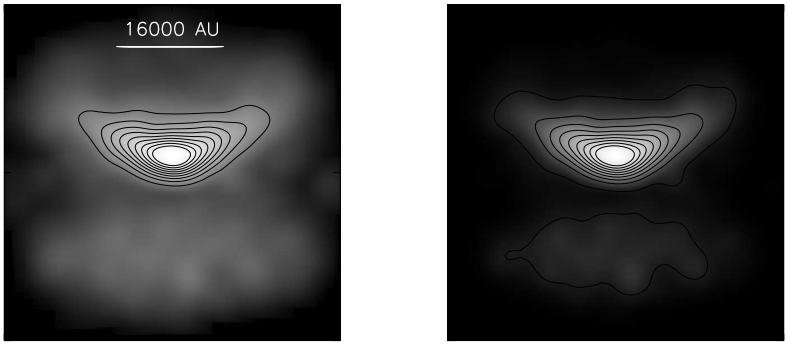

(a) (b)

Fig. 5.— Models of object A at IRAC band 2. Model parameters are: $T_\star = 14000\ K, R_d = 20000\ AU, log(M_d/M_\star) = 1, i = 73°$. Image (a) is convolved with a gaussian, and image (b) is as (a), but with a background of 7% added, which masks the lower level outer regions of the disks improving the model fit. Images have been scaled by a power of 0.3, however each contour represents a 10% drop in surface brightness with the highest contour being 90% of the peak value and the lowest being 10% of the peak value.

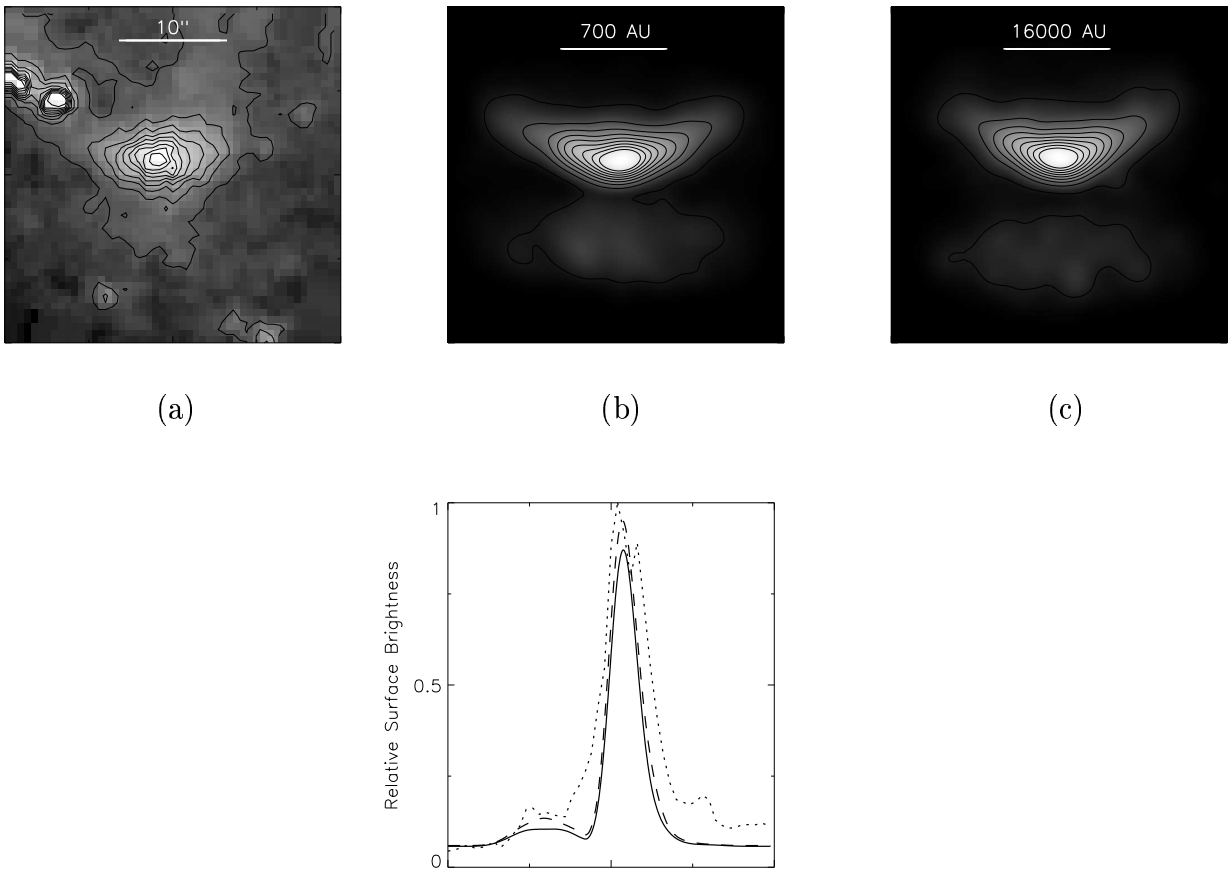

Fig. 6.— Comparison between IRAC band 2 data and models of object A. Image (a) shows a contour plot of the IRAC band 2 data. Contour plots of our 1000AU and 20000AU disks models are shown in (b) and (c) respectively. Image (d) compares a cross-section through the central region of the data and the two models shown in (b) and (c). Model parameters are detailed in Table 2. Images and contours scaled as in Fig. 5. Cross-sections are scaled to the maximum value of the observed data. All models have a background of ∼7% added, which masks the lower level outer regions of the disks improving the model fit. The cross-sections perpendicular to the disk show that relative fall-off in flux is consistent between data (dotted) and models A.1 (dashed), A.2 (solid).

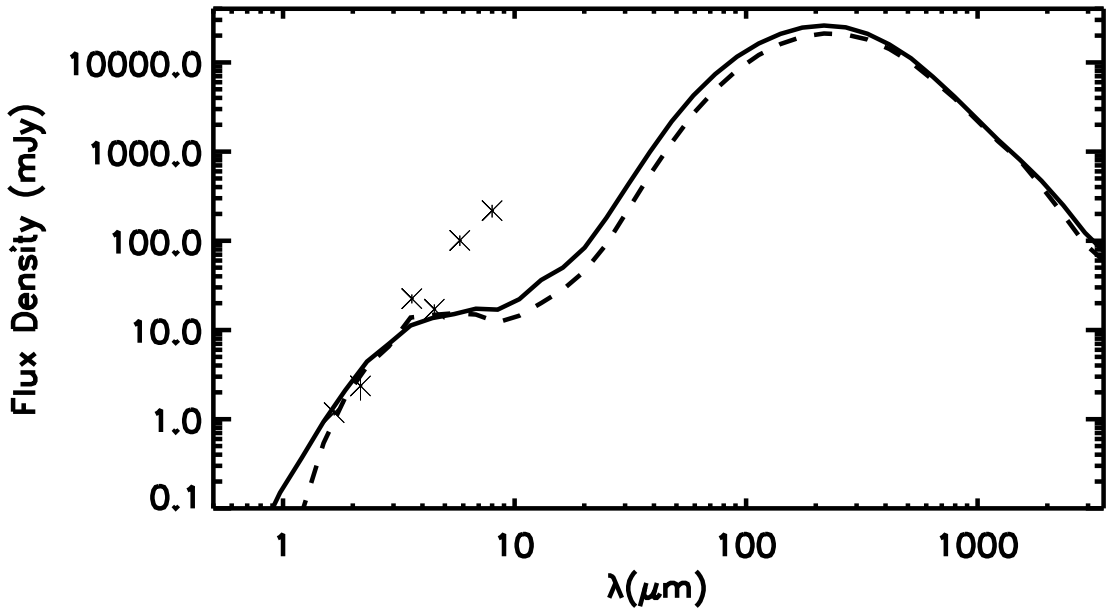

Fig. 7.— The spectral energy distribution (SED) of models A.1 (dashed), A.2 (solid) and the H,K, and IRAC band 1,2,3,4 observations of Object A. J band flux negligible and not plotted. Model SEDs have been reddened according to the empirical relationships from Cardelli et al. (1989) with Rv=4.1 and using $A_\lambda \propto \lambda^{-1.9}$ from Kaas (1999) for $\lambda > 3.5\mu$m. Av=17 and a distance of 70pc applied to model A.1. Av=6.2 and a distance of 1600pc applied to model A.2. These radiative equilibrium models do not fit at IRAC bands 1,3 and 4 possibly due to PAH heating, which we do not account for here.

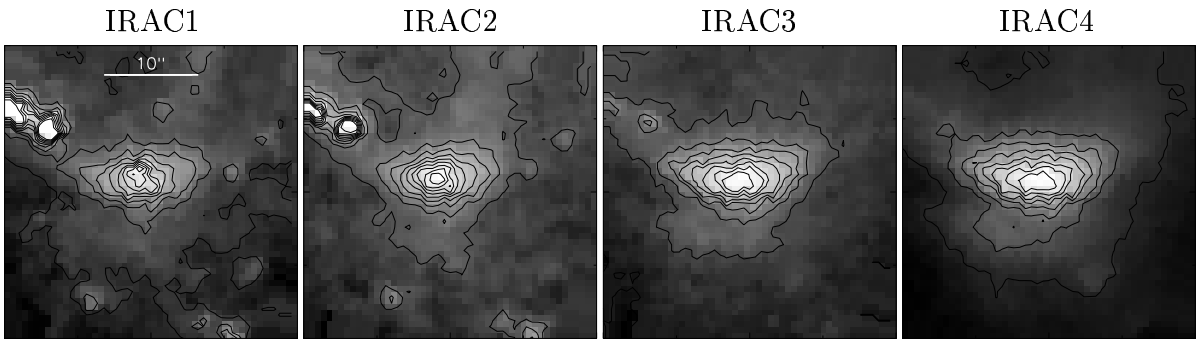

(a)

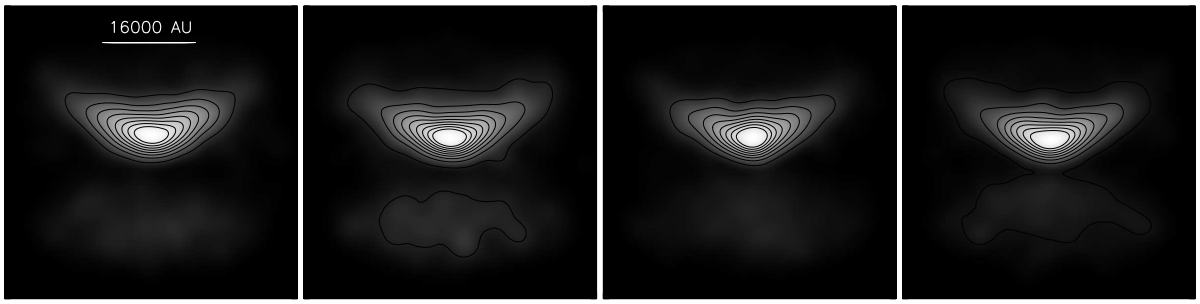

(b)

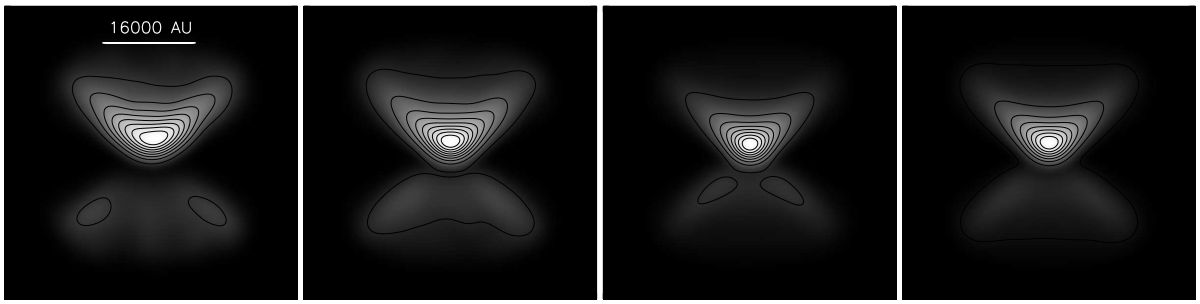

(c)

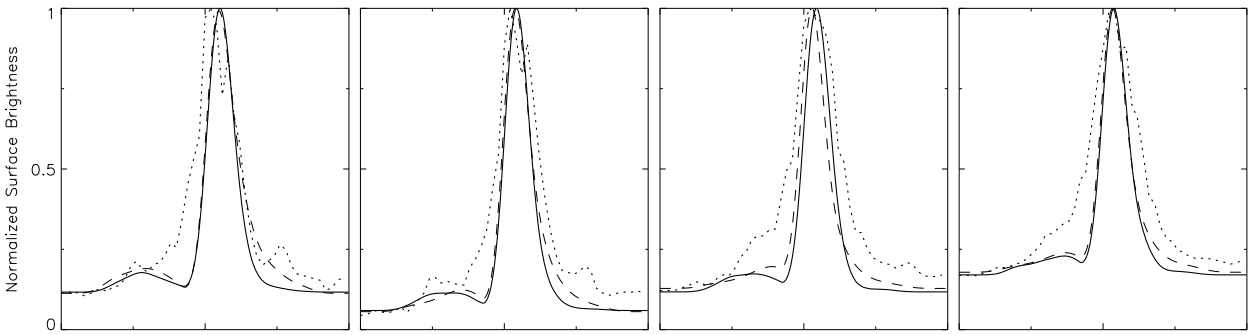

(d)

Fig. 8.— Contoured IRAC band 1,2,3,4 images (a), model A.2 (b), approximate pah model A.3 (c), and (d) cross-sections through the corresponding images (a-dotted),(b-solid) and (c-dashed). All are normalized to the maximum value of each data set and a background applied as in Fig. 5. A.3 images are more flared as the UV optical depth $\tau = 1$ surface is at a larger height above the mid-plane.

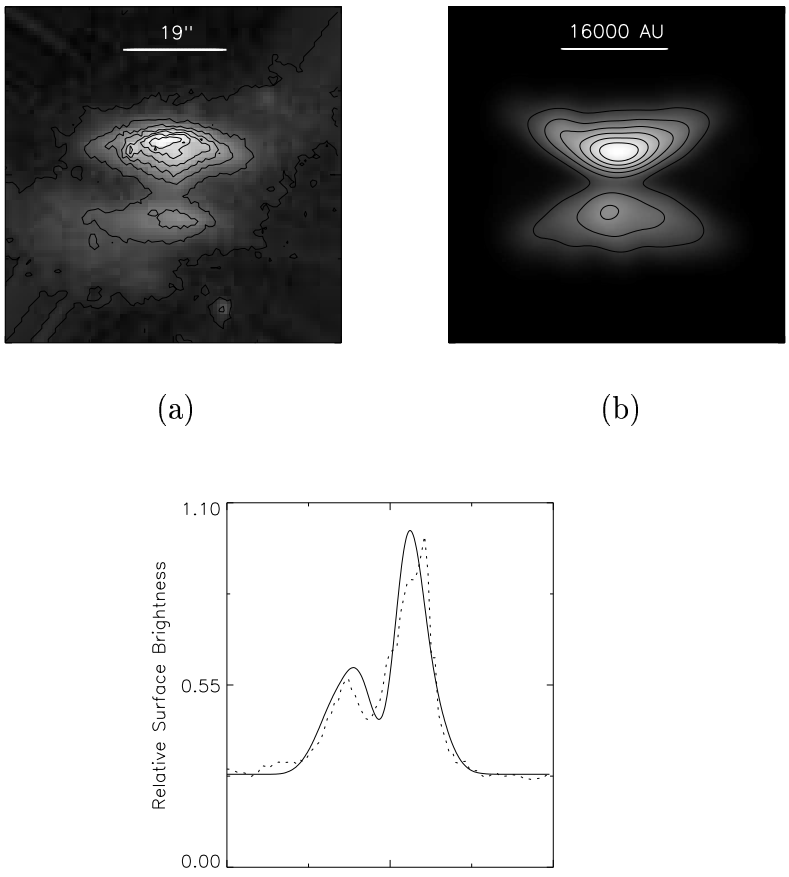

Fig. 9.— Comparison between IRAC band 4 data and model of object B. Image (a) shows a contour plot of the IRAC band 4 data. A contour plots our 20000AU disk model is shown in (b). Image (c) compares a cross-section through the central region of the data and the model shown in (b). Model parameters are detailed in Table 2. Images in the contour plots have been scaled by a power of 0.3, however each contour represents a 10% drop in surface brightness with the highest being 90% of maximum. The cross-sections are scaled to the maximum value of the observed data at IRAC band 4. The model has a background of ∼40% added, which masks the lower level outer regions of the disks improving the model fit. The cross-sections perpendicular to the disk show that relative fall-off in flux is consistent between data and models.